Appl. Phys. B 92, 359–365 (2008)
DOI: 10.1007/s00340-008-3130-3

Applied Physics B
Lasers and Optics

R. CICCHI[1,✉]
L. SACCONI[1]
A. JASAITIS[1]
R.P. O'CONNOR[1]
D. MASSI[2]
S. SESTINI[3]
V. DE GIORGI[3]
T. LOTTI[3]
F.S. PAVONE[1]

Multidimensional custom-made non-linear microscope: from ex-vivo to in-vivo imaging

[1] LENS and Department of Physics, University of Florence, Via Nello Carrara 1, 50019 Sesto Fiorentino, Italy
[2] Department of Human Pathology and Oncology, University of Florence, Viale G.B. Morgagni 85, 50134 Florence, Italy
[3] Department of Dermatology, University of Florence, Via della Pergola 58, 50121 Florence, Italy

Received: 18 January 2008/Revised version: 30 June 2008
Published online: 1 August 2008 • © Springer-Verlag 2008

ABSTRACT We have built a custom-made multidimensional non-linear microscope equipped with a combination of several non-linear laser imaging techniques involving fluorescence lifetime, multispectral two-photon and second-harmonic generation imaging. The optical system was mounted on a vertical honeycomb breadboard in an upright configuration, using two galvo-mirrors relayed by two spherical mirrors as scanners. A double detection system working in non-descanning mode has allowed both photon counting and a proportional regime. This experimental setup offering high spatial (micrometric) and temporal (sub-nanosecond) resolution has been used to image both ex-vivo and in-vivo biological samples, including cells, tissues, and living animals. Multidimensional imaging was used to spectroscopically characterize human skin lesions, as malignant melanoma and naevi. Moreover, two-color detection of two photon excited fluorescence was applied to in-vivo imaging of living mice intact neocortex, as well as to induce neuronal microlesions by femtosecond laser burning. The presented applications demonstrate the capability of the instrument to be used in a wide range of biological and biomedical studies.

PACS 87.64.mn; 78.47.Cd; 87.19.lw

1 Introduction

Two photon microscopy is a laser scanning imaging technique based on a non-linear optical process in which a molecule can be excited by simultaneous absorption of two photons in the same quantum event. The first two photon laser scanning fluorescence microscope was realized in 1990 by Denk, Strickler and Webb [1]. Two photon excitation (TPE) fluorescence microscopy offers an alternative to confocal microscopy that provides many advantages for three-dimensional imaging. Because of the non-linear properties of the excitation, two photon induced fluorescence occurs only at, or near, the focal point of the beam. Long wavelengths, particularly in the near-infrared spectral region, allow deeper penetration in biological materials and are not scattered as much as shorter wavelengths. Optical stacks may be obtained from deeper sections within a tissue that can be achieved by confocal or widefield imaging. In two photon processes the excitation cross section is proportional to the square of the laser intensity. This greatly increases the axial resolution achievable. Two photon excitation eliminates the need of a confocal spatial filter because all the fluorescent light originates from the laser focus spot, giving also higher efficiency. Moreover, photodamage and photobleaching are drastically reduced with respect to confocal and widefield fluorescence imaging.

During the last two decades, the application of TPE microscopy in biological and life sciences has had an impressive growth, above all in biomedical optics and imaging fields. TPE fluorescence microscopy has already been successfully used as a powerful technique for many imaging applications in life science [2, 3]. TPE microscopy has been used in fluorescent proteins investigation and spectroscopy [4, 5] and also to study biological mechanisms inside cells and tissues. Recently, it has also been applied to in-vivo imaging, using common microscopes [6] or combined with optical fibers [7] to realize movable or endoscopic [8] two photon microscopes. Because of the high penetration of the light used, TPE microscopy is particularly useful in human tissues imaging and optical biopsy [9]. Human tissues intrinsically contain many different fluorescent proteins that allow imaging of them without any external added probe. Intrinsic fluorophores, as NADH, keratins, flavins, melanin, elastin, cholecalciferol (vitamin D_3), can be excited by two or three photons excitation, [15] using the Ti:sapphire laser wavelength (typically between 700 and 1000 nm) which is comprised in the optical therapeutic window of tissues.

An immediate implementation for TPE microscopy is represented by second harmonic generation (SHG) microscopy. SHG is a non-linear second-order optical process occurring in materials without a center of symmetry, having a large hyperpolarizability. SHG has already been largely used for imaging non-centrosymmetric molecules inside cells [11], cellular membranes [12, 13], brain [14] and biological tissues [15, 16]. In particular, because of its fibrillar structure, collagen intrinsically has a high hyperpolarizability, providing a high second harmonic contribution and it can be imaged inside connective tissue using SHG microscopy [15, 17]. Recently, SHG mi-

✉ Fax: +39-055-4572451, E-mail: rikka@lens.unifi.it

croscopy was also used for investigating collagen orientation and its structural changes in healthy tissues as human dermis [18, 19] or cornea [20] and also for studying its dynamical modulation in tumors [21, 22].

A further development in fluorescence investigation is represented by the analysis of fluorescence dynamics. Once excited, a population of fluorescent emitting molecules exhibits a fluorescence intensity which exponentially decays in time. Lifetime measurement can yield information on the molecular microenvironment of a fluorescent molecule or on its energy exchanges. Fluorescence lifetime imaging microscopy (FLIM) is a relatively new laser scanning imaging technique. It consists of representing ''pixel-by-pixel'' in the image, the measured fluorescence lifetimes instead of the fluorescence intensities as in traditional laser scanning imaging techniques [23, 24]. FLIM is a useful technique in studying protein localization, protein–protein interaction [25] and fluorescent molecular environment [26]. It has already been used, coupled to TPE, in application involving skin tissue characterization [27, 28] and stratum corneum pH gradient monitoring [29] and coupled to multispectral TPE fluorescence detection in stained samples imaging [30].

2 Experimental setup

We completely designed, built and optimized a custom-made two photon laser scanning fluorescence microscope with two separated detection systems. In the first system, described in Sect. 2.1, the detection is accomplished by photocurrent integration. The second system, based on photon counting regime (Sect. 2.2), is able to perform multispectral fluorescence lifetime imaging microscopy (FLIM) by using a fast 16-channel photomultiplier strip and time correlated single photon counting (TCSPC) detection principle. Microscope calibration, characterization and tests, and imaging of biological samples, are presented in Sect. 3.

The experimental setup (see Fig. 1 for a photo and a schematic drawing) is constituted by a custom-made upright microscope, built to perform two photon laser scanning fluorescence microscopy, second harmonic generation microscopy, conventional wide-field microscopy and fluorescence lifetime imaging microscopy (FLIM) with spectral resolved detection. All the microscope optics are fixed onto a custom vertical honeycomb steel breadboard 60 cm × 90 cm, 070BH0450 (Melles-Griot, NY, US), mounted by two square brackets onto an anti-vibrating optical table 100 cm × 200 cm (TMC, Peabody, MA, US).

For the wide-field subsystem, the light source is a halogen lamp (HL) KL200 (Schott AG, Mainz, Germany) or a custom-made metallic ring with six superluminescent diodes for thin and thick samples, respectively. In both cases the sample image is collected and projected into a color CCD camera COOLPIX 4700 (Nikon, Japan) using a tilting mirror (M5).

Regarding the two photon excitation, a mode-locked Ti:sapphire laser CHAMELEON (Coherent Inc., Santa Clara, CA, US), provides the excitation light, which comprises 120 fs width pulses at a 90 MHz repetition rate, tunable in wavelength between 705 and 980 nm. The laser light beam path includes a collimating telescope (L1, L2), a half wavelength broadband waveplate ($\lambda/2$) coupled with a calcite

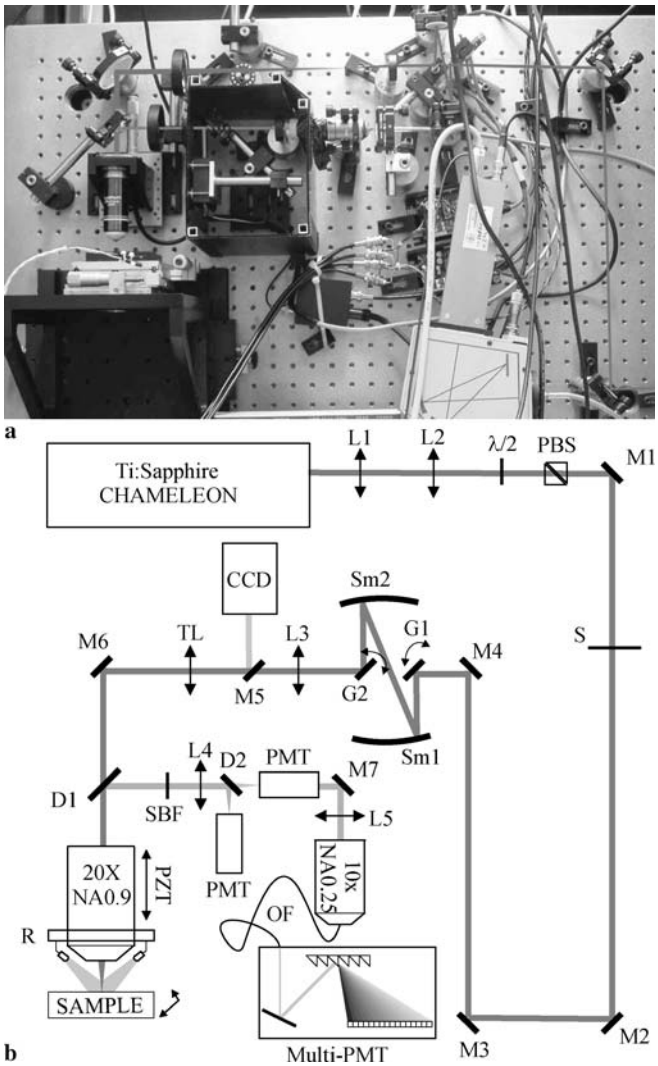

FIGURE 1 A photo (**a**) and a schematic drawing (**b**) of the multidimensional non-linear microscope

polarizing beam splitter (PBS) for laser power adjustment and a custom-made electronic shutter (S), before passing to the scanning head. The scanning head comprises two galvo mirrors (G1, G2) VM500 (GSI Lumonics, Munich, Germany), rotated about orthogonal pivots and coupled by a spherical mirrors pair (Sm1, Sm2). The total dimensions of this scanning head are 100 mm × 180 mm × 150 mm. This solution allowed the mounting of all the optics on the vertical breadboard, as described in paragraph. A small astigmatism effect was introduced in the beam by the spherical mirrors tilting. This effect can be avoided using a supplementary cylindrical lens. Anyway, the measurements performed did not require removal of this spurious effect. The laser beam is raster scanned by opportunely moving the two galvo mirrors, such that the beam focus is scanned in the focal plane of the objective lens with a pixel dwell time of typically 5 s. A scanning lens (L3, $f = 50$ mm) and the microscope tube lens (TL, $f = 200$ mm) expand the beam to a dimension of around 1 cm, before it is focused onto the specimen by an objective XLUM 20, NA 0.90, W.D. 2 mm (Olympus Co., Japan). A piezoelectric stage (PZT) PIFOC P-721

(Physik Instrumente GmbH, Karlsruhe, Germany) allows axial displacements of the objective up to 100 μm with sub-nanometer resolution, and hence the optical sectioning of the sample.

2.1 *Two photon fluorescence detection system*

The detection system for the two photon fluorescence is constituted by a dichroic filter (D1) 685DCXRU (Chroma Technology Corporation, Rockingham, VT, US) with 685 nm cut off wavelength, positioned as close as possible to the objective lens mount. The light path for the fluorescence has to be as short as possible in order to minimize light losses. Fluorescence light is decoupled from the laser path in non-descanning mode. A two photon cut off filter (SBF) E700SP-2P (Chroma Technology Corporation, Rockingham, VT, US) eliminates laser light back reflections. Light passes through a lens (L4) and hits on a dichroic mirror (D2) with 565 nm cut off wavelength, before being focused onto the active area of two photomultiplier detectors (PMT) H7710-13 (Hamamatsu Photonics, Hamamatsu City, Japan). The photocurrent is amplified by a pre-amplifier and integrated using custom-made electronics.

2.1.1 Spatial resolution. In two photon microscopy the spatial resolution depends, as demonstrated in paragraph, on the dimensions of the scanning beam focus. In order to measure the focus dimension we put on a microscope slide a solution containing fluorescent beads of 50 nm diameter. The beads were water-diluted in order to obtain a concentration of less than a bead per scanned field of view.

The optical scanning in the three spatial directions was accomplished using water ($n = 1.33$) as an immersion medium, a laser excitation wavelength of 740 nm, a numerical aperture of the objective of 0.9 and a pixels distance of 19.5 nm (10 μm field dimensions, 512 pixels) and 500 nm along the radial and axial direction, respectively. The distance between two adjacent pixels in X and Y directions was calculated after a calibration with a graded microscope slide. For the same distance along the axial direction, the capacitive position sensor of the piezoelectric PIFOC translator was used. The acquired image stack is represented in Fig. 2a. The fluorescence signal profile was fitted in each direction using a gaussian function as a fitting function, representing the point spread function. The spatial resolution was then measured as the width at half the maximum value (FWHM) of the best fitting function (see Fig. 2). The values obtained for the FWHM, calculated using the formula FWHM $= 2.35\sigma$ were (780 ± 10) nm, (920 ± 6) nm along the X and Y direction, respectively, giving a mean radial resolution of (850 ± 10) nm, and (3.0 ± 0.4) μm along the Z direction.

2.2 *FLIM detection setup*

The fluorescence light collected by the objective is separated from the laser optical path by a dichroic filter (D1) 685DCXRU (Chroma Technology Corporation, Rockingham, VT, US), positioned as close as possible to the objective lens (non-descanning mode). A two photon cut off filter (SBF) E700SP-2P (Chroma Technology Corporation, Rockingham, VT, US) eliminates laser light back reflections. A couple of lens (L4, L5), constituting a telescope, reduces the angle spanned by the fluorescence light during the scanning. An objective lens Plan 10 ×, 0.25 NA (Nikon, Japan) couples the fluorescence light in a multimode optical fiber (OF). The detector (Multi-PMT) PML-Spec (Becker & Hickl GmbH, Berlin, Germany) is constituted by a diffraction grating and a 16-channels multi-anode photomultiplier strip with 200 ps FWHM pulses. It allows spectral resolved (13 nm for each channel) measurements of fluorescence light with variable spectral range. The detection has an upper wavelength limit of 685 nm set by the cut off optical filter, and a lower limit of 200 nm set by the detector response. Acquisition and control are performed using a PC and two synchronized I/O boards, PCI-MIO-16E (National Instruments, Austin, TX, US) and SPC-730 (Becker & Hickl GmbH, Berlin, Germany). The former board controls the movements of the scanning mirrors, whereas the latter is dedicated to time-resolved measurements on each spectral channel. The two boards are synchronized by an electronic timing board E-6502 (National Instruments, Austin, TX, US). The output settings are controlled by a custom-made software developed in LabView ambient.

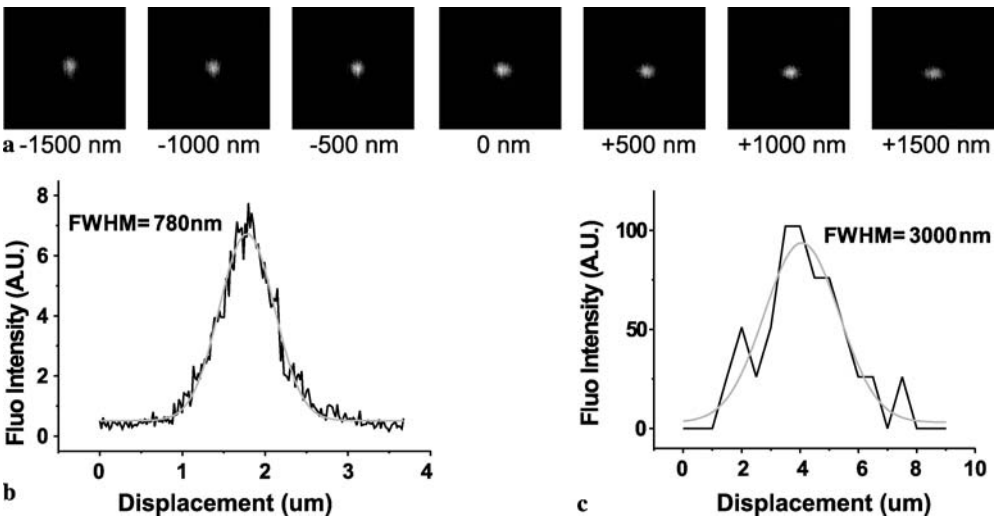

FIGURE 2 Optical axial sectioning of a 50 nm diameter fluorescent bead (**a**). Images have a dimension of 10 μm and a resolution of 512 pixels. The axial displacements are indicated. Radial (**b**) and axial (**c**) measured PSF of the two photon microscope for the bead in (**a**) with superimposed gaussian fits (*grey lines*). The measurement was performed under the following experimental conditions: refractive index of the external medium (water) $n = 1.33$, excitation wavelength $\lambda = 740$ nm, objective numerical aperture NA $= 0.9$

The input settings and the visualization of the acquired images are accomplished using a dedicated software SPCM 1.1 (Becker & Hickl GmbH, Berlin, Germany) that also allows changing of the photon counting board settings. Image pixels exponential fits, image de-convolution and analysis are performed using the software SPC-Image 2.8 (Becker & Hickl GmbH, Berlin, Germany).

2.2.1 Time resolution. Each channel of the multispectral detector provides an output pulse of about 200 ps FWHM (data sheets). As described in the paragraph, the time resolution of a TCSPC system is described by the total instrument response function (IRF), which is in turn the convolution product between the impulse response function of all system elements. In order to measure the IRF of the system, a laser pulse was assumed as an impulse response function. This approximation can be used, because the FWHM of the laser pulse (120 fs) is about three orders of magnitude shorter than the expected FWHM of the IRF. For this measurement, the two photon blocking filter was removed from the fluorescence path and a mirror was put on the laser path between the dichroic filter and the objective lens. In this way, a small fraction of the back-reflected laser light was directed into the fluorescence path, opportunely filtered and collected by the optical fiber into the detector. The recorded detector output pulse is represented in Fig. 3. The FWHM was approximately 300 ps. This value has to be compared with the value of 200 ps of the multispectral detector. The difference between the two values resides in the spreading caused by the other system elements as optical components and electronics. Nevertheless, the measured FWHM of the IRF does not affect time resolution of lifetime measurement if an appropriate de-convolution is performed.

2.3 *Hardware and software*

2.3.1 Proportional regime data acquisition. A PCI-MIO-16E (National Instruments, Austin, TX, US) is used as multifunction data (DAQ) acquisition board. The DAQ board includes: 16 analog input channels at up to 1.25 MS/s of speed (12 bit resolution), 2 analog output channels at up to 1 MS/s of speed (12 bit resolution), and 8 digital I/O lines (TTL/CMOS). Four analog input channels are used to acquire the amplified PMT signals (AI0) and (AI1), and the position monitor of the two galvo mirrors (AI2) and (AI3). The two analog outputs (AO0) and (AO1) are used to drive the two galvo mirrors. A digital line (DIO0) is used to supply a TTL signal which controls the opening of an electronic shutter.

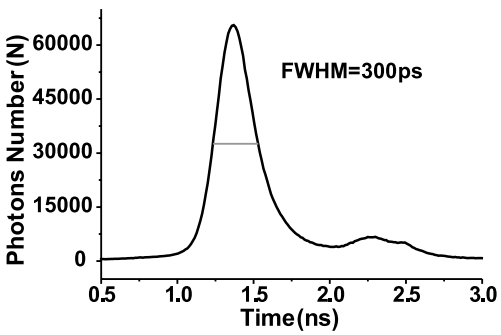

FIGURE 3 Measured IRF of the FLIM system. The measured output pulse is the response to a 120 fs laser pulse centered at 750 nm wavelength

A custom software ImagingXYZ, developed in LabView ambient, generates two different waveforms that drive the galvo mirrors scanning. The waveforms for the galvo-X and for the galvo-Y scanners are a triangular wave and a linear decreasing ramp, respectively. The refreshing rate of the Y waveform is equal to a semi-period of the X triangular waveform. The mixed XY waveform is a raster graph.

The scanning system is made of two galvo mirrors VM500 (GSI Lumonics, Munich, Germany), controlled by two independent single axis servo amplifiers MiniSAX (GSI Lumonics, Munich, Germany). System I/O includes command input, position output and feedback status. The command input to the MiniSAX is a differential input accepting a full-scale command of ± 3 V. The scanner position is provided as differential output with the same scale factor as the command input.

The piezoelectric translator is a PIFOC for microscope objective P-721 (Physik Instrumente GmbH, Karlsruhe, Germany), providing a positioning range of up to 100 μm with sub-nanometer resolution. The amplifier module and the servo-controller are computer interfaced by a microprocessor-controlled interface E-816 (Physik Instrumente GmbH, Karlsruhe, Germany). The output channel is controlled through an analog input channel accepting a voltage range from -2 V to 10 V, or from the computer through the RS-232 interface, controlled through LabView drivers.

The two photosensor modules H7710-13 (Hamamatsu Photonics, Tokyo, Japan) contain two high-voltage power supply circuits and two 13 mm diameter side-on photomultiplier tubes. The photomultiplier tubes have a reflection mode photocatode that delivers high quantum efficiency, an adequate gain of up to 10^7 and fast time response. The signals output are delivered to two amplifiers C6438-01 (Hamamatsu Photonics, Hamamatsu City, Japan) with wide bandwidth (dc to 50 MHz). They provide the voltage output signals with a conversion factor of 25 mV/μA. The signals are processed by two RC low-pass filters which "stretch out" the short pulses of the photosensor modules. The time constant τ of the filters should be chosen to be at least three time smaller than the pixel dwell time of the acquisition. Typical values of the time constant and pixel dwell time are 1 and 5 μs, respectively. The output signals of the RC filters are then buffered by an amplifier and presented to the analog inputs (AI0) and (AI1) of the acquisition board.

The ImagingXYZ software configures the synchronized I/O of the DAQ board. First of all, the output and the input functions are initialized by allocating two memory buffers of the same dimensions (corresponding to the data dimensions of the image to be acquired). The two output waveforms are written on the output memory buffer and a trigger line is configured for simultaneously starting the I/O. Then, the analog output and the analog input are started and one data memory buffer is read on a selected channel of the analog input at the same sampling rate as the analog output. This software can be used in XY or in XYZ mode in order to acquire a single image or a z-stack of images, respectively. In the XY mode, the software requires three different inputs: the number of pixels of the image to be acquired (equal number for X and Y pixels),

the pixel dimension in microns and the sampling rate (equal to the inverse of the pixel dwell time).

2.3.2 Photon counting regime data acquisition. The SPC-730 has an electronic time resolution of 7 ps FWHM and a dead time of 150 ns, allowing a photon count rate up to 8 MHz. The board has two main inputs: a SYNC input, directly connected to the external SYNC of the pulsed laser source, and a CFD input, connected to a preamplified output of the detector. Both inputs accept voltage in the range between 50 mV and 2 V with negative polarity. An additional "routing" input (constituted by 14 lines) is required when using the board with multiple detectors. When used in SCAN-SYNC-IN mode, the board needs three more input signals: a FRAME signal, a LINE clock and a PIXEL clock. The PIXEL clock and the LINE clock are two TTL pulse trains synchronized to the movements of the galvo-X and galvo-Y scanners, respectively. The FRAME signal is a TTL pulse obtained by changing the status of a digital line. These signals are used to fix the position of a single pixel in the scanned image and they are supplied by the timing board E-6602 (National Instruments, Austin, TX, US), used to synchronize the DAQ acquisition board with the single photon counting module. The timing board includes: 8 digital TTL counter/timer, 32 bit resolution, internal timebase with selectable values of 100 kHz, 20 MHz, and 80 MHz. Two couples of counters are used in start-stop mode in order to generate two different trains of pulses. The first pulse train is the PIXEL clock, synchronized with the movements of the galvo-X mirror. The second pulse train is the LINE clock, synchronized with the movements of the galvo-Y mirror. The synchronization with the scanners movements is accomplished using an external trigger line, connecting the E-6602 with the PCI-MIO-16E board. The PIXEL and the LINE clocks are presented to two separated input lines of the photon counting module.

The PML-Spec (Becker & Hickl GmbH, Berlin, Germany) contains a polychromator and a 16 channel detector head. The polychromator is composed by a diffraction grating, with 600 lines/mm which can operate in the 300–850 nm spectral range, and two mirrors. It is optically connected to the fluorescence path through a multimode optical fiber. The total spectral range detectable by the 16 channels detector head is 208 nm (13 nm for each channel). A micrometer translator allows fine displacements of the diffraction grating and hence the variation of the detected wavelength range. The PML-16 detector head contains a multi-anode PMT R-5900-L16 (Hamamatsu Photonics, Hamamatsu City, Japan) in a linear geometry and the routing electronics for the 16 detector channels. The output pulse has an average temporal width of 200 ps FWHM and an average amplitude of 40 mV with negative polarity. Output pulses are presented to the CFD input of the photon counting module through a coaxial cable with SMA connectors. Another output supplies the "routing" signal to the photon counting module to which it is directly connected through a cable with a sub-D 15-pin connector. The detector requires an external high-voltage power supply PS310 (Stanford Research Systems, Sunnyvale, CA, US), giving a programmable high voltage output in the range from 50 to 1250 V with selectable polarity and 1 V resolution, and a maximum output current of 20 mA. The output settings used for supplying the multi-anode detector are -900 V/0.35 mA.

A custom software FLIMImaging, working simultaneously with SPCM 1.1 software, drives the movements of the two galvo scanners and generates the scan control signals (FRAME signal, LINE clock, PIXEL clock) required by the single photon counting module. The software requires five different input settings: the number of X and Y pixels to be scanned, the pixel dwell time in microseconds, the dimensions of one pixel and the duty ratio of the two trains of TTL pulses, corresponding to the LINE clock and PIXEL clock signal. First of all, the software enables two couples of digital counters on the timing board by changing the status of a digital line. Then, it executes in a sequence the raster generation software, and the synchronized I/O software to check scanners position.

3 Applications

3.1 *Ex-vivo lifetime imaging of malignant melanoma (MM) and melanocytic naevus (MN)*

Lifetime analysis with FLIM was applied to malignant melanoma (MM) and melanocytic nevus (MN) imaging. In multiphoton imaging, the MN or MM sample has been cut, maintaining both healthy skin and lesion, to obtain a regular shape, allowing its positioning either with the skin surface parallel to the optical axis (horizontal optical sectioning), or perpendicular (vertical optical sectioning). Before observation, the investigated samples have been included in a 4% agarose gel in order to prevent unwanted movements during observation. A saline solution has been used as an immersion medium for the objective lens in order to maintain the natural tissue osmolarity. Samples were imaged with non-linear microscopy within the same day of excision. In this case we imaged two ex-vivo sample of both malignant melanoma, and melanocytic naevus. In particular, we evaluated the lifetime distribution using double-exponential decay analysis of a layer containing MM or MN cells. Lifetime distributions were calculated by averaging the lifetime distribution acquired inside five different images containing MM cells. For the purpose of comparison, the same averaging calculation was performed for layers of MN cells. Fluorescence decays were fitted using a double-exponential decay function. For double-exponential decay we analyzed both the mean lifetime distribution, and the separated fast and slow components distribution. Figure 4 shows the lifetime comparisons between MM and MN. In particular, we found that MM and MN have different lifetime distributions. MM exhibited a broader mean lifetime distribution with respect to the corresponding MN mean lifetime distribution. However, the mean lifetime distribution is ranging the same values for both MM and MN. Two particular images for MM (Fig. 4a) and for MN (Fig. 4b) are plotted in Fig. 4. The two images represent a TPE fluorescence intensity image of a selected cellular layer. The corresponding graphs for the averaged data on MM, and MN are plotted in Fig. 4c–e, for the double-decay mean lifetime, fast lifetime component and slow lifetime component, respectively. By separating the two slow and fast lifetime components, we measured a similar slow lifetime distribution for MM and MN (Fig. 4e), whereas we measured different fast lifetime distributions (Fig. 4d), so that the differentia-

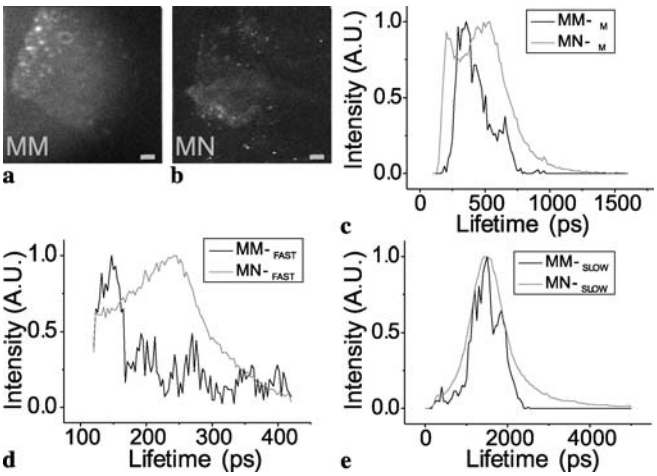

FIGURE 4 TPE fluorescence intensity image acquired by a photon counting method for MM (**a**), and MN (**b**). Field of view: 150 μm. *Scale bars*: 15 μm. The corresponding averaged lifetime distributions are plotted in *black* (MM), and *grey* (MN) in the *graphs at the bottom* for double-decay mean lifetime (**c**), double-decay fast lifetime component (**d**), and double-decay slow lifetime component (**e**). The lifetime distributions presented were all normalized to their maximum value

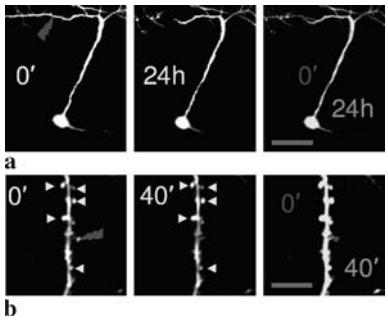

FIGURE 5 In-vivo multi-photon nanosurgery. (**a**) Overlay of maximum-intensity *z*-projections (from 500 to 100 μm depth) of a layer-5 pyramidal neuron before (0′) and 24 h after (24h) dendritic dissection (as indicated by the *lightning symbol*). The merge on the *right* shows the integrity of the remaining structure after dissection. The dendrite was irradiated just after the acquisition of the first image. *Scale bar*: 60 μm. (**b**) Time-lapse images of a section of the dendrite where several spines are present. The single spine indicated by the *lightning symbol* was irradiated just after the acquisition of the first image. The *arrowheads* highlight the stability of the surrounding dendritic spines. The *panel on the right* shows an overlay of a pair of images from the sequence. The first image acquired at $t = 0'$ and the other one at $t = 40'$. This panel emphasizes the spine stability and the absence of any swelling in the dendrite. *Scale bar*: 15 μm. Adapted from [34]

tion between MM and MN occurs at fast lifetime component level.

3.2 *In-vivo multi-photon nanosurgery on cortical neurons*

In combination with fluorescent protein expression techniques, two-photon microscopy has become an indispensable tool to image cortical plasticity in living mice [31]. In parallel to its application in imaging, multi-photon absorption has also been used as a tool for the selective disruption of cellular and intracellular structures [32, 33]. Our group demonstrated a method for performing multi-photon nanosurgery in the central nervous system of mice [34].

We exploited the spatial localization and deep penetration of multi-photon excitation to perform selective lesions on the neuronal processes of cortical neurons in mice expressing fluorescent proteins (YFP H-line and GFP M-line). Neurons were irradiated with a focused, controlled dose of femtosecond laser energy delivered through a cranial optical window [7].

In a first series of experiments, this methodology was applied to irradiate a single dendrite in the parietal cortex. Briefly, we found that the morphological consequences of irradiating a single dendrite can be grouped into two categories of response: 1) transient swelling with recovery and 2) complete dendritic dissection. In the former case, we observed a swelling of the dendrite extending 5–25 μm from the point of irradiation along the dendrite in both directions. The spines present on the irradiated dendrite temporarily disappeared with the swelling, but returned after a period of minutes to hours with the original shape of the dendrite. In the latter class of responses, the dendrite was completely severed. As shown in Fig. 5a, after laser irradiation the terminal end of the dendrite distal to the dissection point followed a sequence of swelling, degeneration and disappearance. We can clearly observe (Fig. 5b) that the portion of dendrite no longer attached to the soma disappears. The spatial localization of multi-photon nanosurgery was maximally demonstrated by the ablation of individual dendritic spines. As clearly shown in Fig. 5b, we were able to remove a single dendritic spine without causing any visible collateral damage to the adjacent spines or to the parent dendrite.

The combination of multi-photon nanosurgery and in-vivo imaging represents a promising tool for probing and disrupting neuronal circuits. The potential of using this precise optical method to perturb individual synapses cannot be overstated. Using multi-photon nanosurgery, the synaptic organization of the brain can now be teased apart in-vivo to understand micro-circuitry, in the same way that chemical and electrical ablation methods linked brain and behaviour in the previous century.

4 Conclusion

In this paper, we have presented and described in detail a custom-made multidimensional non-linear microscope, designed to be used in several ex-vivo and in-vivo biomedical applications. The measured spatial ((780 ± 10) nm, and (3.0 ± 0.4) μm for radial and axial, respectively) and time (FWHM of the IRF of 300 ps) resolutions are enough to perform both two photon fluorescence imaging and fluorescence lifetime imaging microscopy on both ex-vivo and in-vivo samples. The presented tests on human skin tissue samples with malignant melanoma and melanocytic naevus, and on in-vivo imaging on living mice were shown, so demonstrating all the setup capabilities, including nanosurgery. This setup can be used in multiple non-linear imaging application ranging from ex-vivo to in-vivo.

REFERENCES

1 W. Denk, H.J. Strickler, W.W. Webb, Science **248**, 73 (1990)
2 K. König, J. Microsc. **200**, 83 (2000)

3 W.R. Zipfel, R.M. Williams, W.W. Webb, Nat. Biotechnol. **21**, 1369 (2003)
4 C. Xu, W. Zipfel, J.B. Shear, R.M. Williams, W.W. Webb, Proc. Nat. Acad. Sci. USA **93**, 10 763 (1996)
5 S. Huang, A.A. Heikal, W.W. Webb, Biophys. J. **82**, 2811 (2002)
6 J. Peti-Peterdi, S. Morishima, P.D. Bell, Y. Okada, Am. J. Physiol. Renal Physiol. **283**, F197 (2002)
7 F. Helmchen, D.W. Tank, W. Denk, Appl. Opt. **41**, 2930 (2002)
8 M.T. Myaing, D.J. MacDonald, X. Li, Opt. Lett. **31**, 1076 (2006)
9 B.R. Masters, P.T.C. So, E. Gratton, Lasers Med. Sci. **13**, 196 (1998)
10 W.R. Zipfel, R.M. Williams, R. Christie, A.Y. Nikitin, B.T. Hyman, W.W. Webb, Proc. Nat. Acad. Sci. USA **100**, 7075 (2003)
11 A. Zoumi, A.T. Yeh, B.J. Tromberg, Proc. Nat. Acad. Sci. USA **99**, 11 014 (2002)
12 L. Moreaux, O. Sandre, J. Mertz, J. Opt. Soc. Am. B **17**, 1685 (2000)
13 L. Sacconi, M. D'Amico, F. Vanzi, T. Biagiotti, R. Antolini, M. Olivotto, F.S. Pavone, J. Biomed. Opt. **10**, 024 014 (2005)
14 D.A. Dombeck, K.A. Kasischke, H.D. Vishwasrao, M. Ingelsson, B.T. Hyman, W.W. Webb, Proc. Nat. Acad. Sci. USA **100**, 7081 (2003)
15 W.R. Zipfel, R.M. Williams, R. Christie, A.Y. Nikitin, B.T. Hyman, W.W. Webb, Proc. Nat. Acad. Sci. USA **100**, 7075 (2003)
16 P.J. Campagnola, A.C. Millard, M. Terasaki, P.E. Hoppe, C.J. Malone, W.A. Mohler, Biophys. J. **81**, 493 (2002)
17 R.M. Williams, W.R. Zipfel, W.W. Webb, Biophys. J. **88**, 1377 (2005)
18 Y. Sun, W.L. Chen, S.J. Lin, S.H. Jee, Y.F. Chen, L.C. Lin, P.T.C. So, C.Y. Dong, Biophys. J. **91**, 2620 (2006)
19 R. Cicchi, S. Sestini, V. De Giorgi, D. Massi, T. Lotti, F.S. Pavone, J. Biophoton. **1**, 62 (2008)
20 M. Han, G. Giese, J.F. Bille, Opt. Express **13**, 5791 (2005)
21 E.B. Brown, T.D. McKee, E. Di Tomaso, A. Pluen, B. Seed, Y. Boucher, R.K. Jain, Nat. Med. **9**, 796 (2003)
22 S.J. Lin, S.H. Jee, C.J. Kuo, R.J. Wu, W.C. Lin, J.S. Chen, Y.H. Liao, C.J. Hsu, T.F. Tsai, Y.F. Chen, C.Y. Dong, Opt. Lett. **31**, 2756 (2006)
23 P.I.H. Bastiaens, A. Squire, Trends Cell. Biol. **9**, 48 (1999)
24 W. Becker, A. Bergmann, C. Biskup, L. Kelbauskas, T. Zimmer, N. Klöcker, K. Benndorf, Proc. SPIE **4963**, 175 (2003)
25 R.R. Duncan, A. Bergmann, M.A. Cousins, D.K. Apps, M.J. Shipston, J. Microsc. **215**, 1 (2004)
26 S.Y. Breusegem, M. Levi, N.P. Barry, Nephron Exp. Nephrol. **103**, e41 (2006)
27 K. König, I. Riemann, J. Biomed. Opt. **8**, 432 (2003)
28 R. Cicchi, D. Massi, S. Sestini, P. Carli, V. De Giorgi, T. Lotti, F.S. Pavone, Opt. Express **15**, 10 135 (2007)
29 K.M. Hanson, M.J. Behne, N.P. Barry, T.H. Mauro, E. Gratton, R.M. Clegg, Biophys. J. **83**, 1682 (2002)
30 D.K. Bird, K.W. Eliceiri, C.H. Fan, J.G. White, Appl. Opt. **43**, 5173 (2004)
31 J.T. Trachtenberg, B.E. Chen, G.W. Knott, G. Feng, J.R. Sanes, E. Welker, K. Svoboda, Nature **420**, 788 (2002)
32 J.A. Galbraith, M. Terasaki, Mol. Biol. Cell. **14**, 1808 (2003)
33 I.M. Tolic-Norrelykke, L. Sacconi, G. Thon, F.S. Pavone, Curr. Biol. **14**, 1181 (2004)
34 L. Sacconi, R.P. O'Connor, A. Jasaitis, A. Masi, M. Buffelli, F.S. Pavone, J. Biomed. Opt. **12**, 050 502 (2007)
35 F. Helmchen, W. Denk, Nat. Methods **2**, 932 (2005)